AIMS Mathematics, 10(6): 13855–13879.
DOI: 10.3934/math.2025624
Received: 05 March 2025
Revised: 19 May 2025
Accepted: 23 May 2025
Published: 17 June 2025

https://www.aimspress.com/journal/Math

Research article

Numerical approximation for solving time-fractional Benjamin-Bona-Mahony-Burger model via cubic B-spline functions

Muserat Shaheen[1], Muhammad Abbas[1,*], Miguel Vivas-Cortez[2,*], M. R. Alharthi[3] and Y. S. Hamed[3]

[1] Department of Mathematics, University of Sargodha, 40100 Sargodha, Pakistan

[2] Faculty of Exact, Natural and Environmental Sciences, Pontificia Universidad Católica del Ecuador, FRACTAL (Fractional Research in Analysis, Convexity and Their Applications Laboratory), Av 12 de octubre 1076 y Roca, Apartado Quito 17-01-2184, Ecuador

[3] Department of Mathematics and Statistics, College of Science, Taif University, P. O. Box 11099, Taif 21944, Saudi Arabia

* **Correspondence:** Email: muhammad.abbas@uos.edu.pk, mjvivas@puce.edu.ec.

Abstract: Many years of research have gone into spline functions, and they are now used in countless computational tasks. Splines have a lot of useful properties that make them an excellent tool for numerical problem solving, which account for their never-ending applications. The piecewise continuous functions known as spline functions yield smooth outcomes. The numerical solution to the nonhomogeneous time-fractional Banjamin-Bona-Mahony-Burger problem was presented in this study. The objective of the study was to obtain accurate numerical results by applying the Atangana-Baleanu fractional derivative with the help of the forward difference scheme for integer-order time derivative while the θ-weighted scheme with the collaboration of cubic B-spline functions was used for the spatial derivatives. The stability of the proposed scheme was analyzed and proved to be unconditionally stable. The convergence analysis was also studied, and it was of the second order $O(h^2 + (\Delta s)^2)$. The proposed scheme was applicable and accurate, as demonstrated by numerical examples and their conceivable outcomes. The proposed scheme provided accuracy compared to other numerical techniques because it yielded numerical solutions in C^2 continuous piecewise form at each knot in the domain.

Keywords: BBM-Burger equation; cubic B-spline functions; 2nd order accuracy; finite difference techniques; stability; convergence; conclusion
Mathematics Subject Classification: 34G20, 35A20, 35A22, 35R11

1. Introduction

It is well-established that fractional derivatives offer greater flexibility and accuracy compared to integer-order derivatives, particularly when modeling nonclassical engineering and scientific phenomena. Examples include fractional-order recurrent neural networks and various dynamical topics, as discussed in [1], a new extension of the fractality concept introduced in financial mathematics by Laskin et al. [2], frequency dependance of cell rheological behavior studied in [3], and the HIV/AIDS model and the present scenario of COVID-19 discussed in [4, 5]. Fractional derivatives enable accurate modeling of systems requiring accurate modeling of damping. Numerous examples demonstrate the superiority of fractional calculus over integer-order calculus in such applications. Examples illustrating the application of fractional derivatives include: modeling non-linear earthquake fluctuations and developing fluid dynamic traffic models that mitigate problems caused by high traffic flow [6, 7]. Numerous mathematical equations are increasingly being formulated as fractional partial differential equations, finding applications in diverse fields such as mathematical biology, transport, finance, visco-elasticity, particle chemistry, and population dynamics [8–10]. Wave breaking models have two most important equations, which are Kortewegde Varies (KdV) and the Banjamin-Bona-Mahony-Burger (BBM-Burger) equation [11]. In mathematics, KdV is a model of wave and shallow water surface. These equations are not applicable to certain long-wave physical systems, which led to the introduction of the BBM-Burger equations. The BBM-Burger equations serve as a refinement of the KdV equations. Specifically, the integer-order nonlinear BBM-Burger equation, which accounts for both dissipative and dispersive effects, is presented in [12].

The BBM-Burger equations have numerous applications across various fields, including cracked rock, acoustic-gravity waves in fluids, acoustic waves in a harmonic crystal, and thermodynamics [13]. Several methods have been proposed to solve fractional partial-integro differential equations and fractional differential equations, including finite element method with cubic B-spline (CBS) functions for numerical solutions of Burger and Fisher equations [14], CBS collocation method for numerical solutions of nonlinear inhomogeneous time-fractional (TF) Burger-Huxley equations [15], CBS functions for solving TF diffusion equations involving Caputo-Fabrizio fractional derivatives [16], and Atangana-Baleanu fractional derivative (ABFD) with CBS functions for solving TF Burger's equations [17]. Many fractional equations have been solved by using the quartic B-spline collocation method [18], an extended CBS technique [19], shifted Legendre polynomials involved in orthogonal basis function method [20, 21], homotopy analysis method [22], and the fifth-kind Chebyshev polynomial collocation method [23]. For discussing dynamic physical structures, a nonhomogeneous fractional BBM-Burger model with a nonlocal viscous term is proposed [24],

$$v_s + v_{\mathfrak{u}} - \phi v_{\mathfrak{u}\mathfrak{u}s} + \rho^{\psi} D_s^{\psi} v + \tau v v_{\mathfrak{u}} - \chi v_{\mathfrak{u}\mathfrak{u}} = g(\mathfrak{u}, s), \quad s \in [0, S], \ \mathfrak{u} \in [\mathfrak{a}, \mathfrak{b}], \ 0 < \psi \leq 1, \quad (1.1)$$

with initial condition (IC) and boundary conditions (BCs)

$$\begin{cases} v(\mathfrak{u}, 0) = v_0(\mathfrak{u}), \\ v(\mathfrak{a}, s) = f_1(s), \ v(\mathfrak{b}, s) = f_2(s), \end{cases} \quad (1.2)$$

where τ, ϕ, ρ and χ are positive parameters. Due to the complexity of the nonhomogeneous BBM-Burger equation, finding an analytical solution is often challenging. Consequently, recent studies have

focused on developing numerical methods to solve this equation, exploring alternative approaches to approximate its solution. Linearized difference schemes for the BBM-Burger equation incorporating a fractional nonlocal viscous term have been investigated in [25]. The homotopy analysis method was employed to investigate the BBM-Burger equation by Fakhari [26]. Song et al. [27] obtained an approximate solution for the fractional BBM-Burgers equation using the homotopy analysis method. Kumar et al. [28] solved non-integer order BBM-Burger equations using the novel homotopy analysis transform method. Shakeel et al. [29] obtained the exact solution of fractional BBM-Burger equation by using the (G'/G) expansion method. The generalized Atangana-Baleanu BBM-Burgers equation involving dissipative term has been solved by using the modified sub-equation method and new $G'/(bG' + G + a)$ expansion schemes [30]. The residual power series technique for the series solution of the TF BBM-Burger equation has been used by Zhang et al. [31]. Salih et al. [32] applied cubic trigonometric B-spline functions to solve the BBM-Burger equation. A hybrid numerical technique has been used to solve the BBM-Burger equation in [33]. Karakoc et al. [34] obtained the exact traveling wave solution and computational solutions of the BBM-Burger equation by using the modified Kudryashov method and septic B-spline finite element method, respectively. Omrani [35] employed the Crank-Nicolson finite difference method to obtain a numerical solution for the BBM-Burger equation. Karakoc et al. [36] applied the CBS finite element method, in conjunction with a lumped Galerkin scheme, to spatially approximate the solitary-wave solution of the nonlinear BBM-Burger equation. Majeed et al. [37] employed the Caputo fractional derivative and CBS functions to solve the nonhomogeneous TF BBM-Burger equation. Lin et al. suggested an iterative RBF-based approach in order to solve the nonlinear TF BBM-Burger equation in any domain [38]. Mohsin Kamran et al. solved the BBM-Burger equation numerically using Caputo derivative and B-spline basis functions in [39]. Hamad Salih [40] solved the one-dimensional nonlinear BBM-Burger problem using the novel quartic trigonometric B-spline method based on finite difference. Lalit Mohan and Amit prakash provided a very effective method for analyzing the diffusion wave equation and the fractional BBM-Burger equation in [41]. Vineesh Kumar used the ansatz method and Adomian decomposition method on the BBM-Burger equation in [42]. Atallah El-shenawy et al. [43] uses the collocation approach, which is based on the cubic trigonometric B-Spline methodology, to numerically investigate Troesch's problem. Atallah El-shenawy et al. [44] developed a numerical method based on B-spline to solve the time-dependent Emden-Fow-ler-type equations.

The given study is inspired by recent developments in the investigation of computational solution of the nonhomogeneous time-fractional BBM-Burger equation. The objective of this study is to apply the θ-weighted scheme with CBS functions to the nonhomogeneous BBM-Burger equation for obtaining the numerical solution. In the past, many researchers have used B-spline techniques to solve non-homogeneous BBM-Burger equations. However, no one has ever used the CBS method together with the ABFD on the TF term involved in the BBM-Burger equation. The usage of non-singular kernel operator in B-spline methods is novel. Convergence and stability of the proposed problem are analyzed. By presenting few numerical examples, the efficiency and applicability of the proposed scheme is also analyzed. By contrasting analytical and numerical solutions, one can find that the present approach has provided the more effective results. The present scheme is novel for the approximate solution of the nonhomogeneous time-fractional BBM-Burger equation involving ABFD, and, as far as authors are aware, it has never been employed for this purpose before.

This paper has been presented in this way: Basic definitions utilized in this work are given in Section 2. This section contains an important definition of ABFD, which is the core of our work. Section 3 contains the description of the proposed method. Section 4 gives the answer of "how to get the values of the initial vector". Stability and convergence of this problem are given in Sections 5 and 6, respectively. Section 7 contains numerical examples and their discussions. Concluding remarks are presented in Section 8.

2. Basic definitions

The fundamental definitions including the ABFD with several properties [45] are a part of this section.

Definition 1. *The ABFD of order ψ and $v \in H'(0,1)$ is defined as [46]:*

$$\mathcal{D}_s^{\psi} v(\mathfrak{u}, s) = \frac{J(\psi)}{1-\psi} \int_0^s \frac{\partial^n}{\partial c^n} v^n(\mathfrak{u}, c) E_{\psi}\left(\frac{-\psi}{n-\psi}(s-c)^{\psi}\right) dc, \qquad \mathfrak{n} - 1 < \psi \leq \mathfrak{n},$$

where $E_{\psi}(v)$ is the Mittag-Leffler function given as:

$$E_{\psi}(v) = \sum_{\kappa=0}^{\infty} \frac{v^{\kappa}}{\Gamma(\psi\kappa + 1)},$$

and the standardization function $J(\psi)$ can be described as:

$$J(\psi) = 1 - \psi + \frac{\psi}{\Gamma(\psi)}.$$

For $0 < \psi \leq 1$, it becomes

$$\mathcal{D}_s^{\psi} v(\mathfrak{u}, s) = \frac{J(\psi)}{1-\psi} \int_0^s \frac{\partial}{\partial c} v'(\mathfrak{u}, c) E_{\psi}\left(\frac{-\psi}{1-\psi}(s-c)^{\psi}\right) dc, \ 0 < \psi \leq 1. \tag{2.1}$$

Definition 2. *If $\hat{q} \in L^2[\mathfrak{a}, \mathfrak{b}]$, Parseval's identity is given as [47]:*

$$\sum_{\acute{n}=-\infty}^{\infty} |\tilde{q}(\acute{n})|^2 = \int_{\mathfrak{a}}^{\mathfrak{b}} |\hat{q}(r)|^2 dr,$$

where $\tilde{q}(\acute{n}) = \int_{\mathfrak{a}}^{\mathfrak{b}} \hat{q}(r) e^{2\pi i \acute{n} r}$ is the Fourier transform for every integer $\acute{n}$.

2.1. Basis functions

The spatial domain $[\mathfrak{a}, \mathfrak{b}]$ is partitioned as $\mathfrak{a} = \mathfrak{u}_0 < \mathfrak{u}_1 < \cdots < \mathfrak{u}_{\hat{N}} = \mathfrak{b}$, where $\mathfrak{u}_j = \mathfrak{u}_0 + jh,\ j = 0(1)\hat{N}$. Domain is divided into $\hat{N}$ equal subintervals of length $h = \frac{\mathfrak{b}-\mathfrak{a}}{\hat{N}}$. Now, assume that $\Psi(\mathfrak{u}, s)$ is the CBS approximation for $v(\mathfrak{u}, s)$ s.t.

$$\Psi(\mathfrak{u}, s) = \sum_{j=-1}^{\hat{N}+1} y_j^{\hat{n}}(s) F_j(\mathfrak{u}), \tag{2.2}$$

where $F_j(\mathrm{u})$ are CBS functions and $y_j^{\hat{m}}$ are control points that will be computed at each time interval. The CBS functions are defined as [48]:

$$F_j(\mathrm{u}) = \frac{1}{6h^3}\begin{cases}(\mathrm{u}-\mathrm{u}_{j-2})^3, & \mathrm{u}\in[\mathrm{u}_{j-2},\mathrm{u}_{j-1}),\\ h^3+3h^2(\mathrm{u}-\mathrm{u}_{j-1})+3h(\mathrm{u}-\mathrm{u}_{j-1})^2-3(\mathrm{u}-\mathrm{u}_{j-1})^3, & \mathrm{u}\in[\mathrm{u}_{j-1},\mathrm{u}_j),\\ h^3+3h^2(\mathrm{u}_{j+1}-\mathrm{u})+3h(\mathrm{u}_{j+1}-\mathrm{u})^2-3(\mathrm{u}_{j+1}-\mathrm{u})^3, & \mathrm{u}\in[\mathrm{u}_j,\mathrm{u}_{j+1}),\\ (\mathrm{u}_{j+2}-\mathrm{u})^3, & \mathrm{u}\in[\mathrm{u}_{j+1},\mathrm{u}_{j+2}),\\ 0, & \text{otherwise.}\end{cases} \tag{2.3}$$

Domain for time $[0, S]$ can break using knots $0 = s_0 < s_1 < \cdots < s_{\hat{M}} = S$ in $\hat{M}$ uniform subintervals $[s_{\hat{m}}, s_{\hat{m}+1}] : s_{\hat{m}} = \hat{m}\Delta s,\ \hat{m} = 0, 1, \cdots, \hat{M}$, where $\Delta s = S/\hat{M}$ implements numerical scheme. The values of Ψ, Ψ_{u}, and Ψ_{uu} at nodal points can be expressed in terms of the parameter y_j by combining Eq (2.2) with expression $F_j(\mathrm{u})$. These values are summarized in the following Table 1:

Table 1. Values of $(\Psi)_j^{\hat{m}}$, $(\Psi_{\mathrm{u}})_j^{\hat{m}}$, and $(\Psi_{\mathrm{uu}})_j^{\hat{m}}$ at the knots.

	y_{j-1}	y_j	y_{j+1}	Otherwise
$(\Psi)_j^{\hat{m}}$	$\frac{1}{6}$	$\frac{4}{6}$	$\frac{1}{6}$	0
$(\Psi_{\mathrm{u}})_j^{\hat{m}}$	$-\frac{1}{2h}$	0	$\frac{1}{2h}$	0
$(\Psi_{\mathrm{uu}})_j^{\hat{m}}$	$\frac{1}{h^2}$	$-\frac{2}{h^2}$	$\frac{1}{h^2}$	0

3. Description of the method

The ABFD used in (1.1) is discretized at $s = s_{\hat{m}+1}$ as [49]:

$$\frac{\partial^{\psi}}{\partial s^{\psi}}v(\mathrm{u}, s_{\hat{m}+1}) = \frac{J(\psi)}{1-\psi}\sum_{\zeta=0}^{\hat{m}} l_{\zeta}[v(\mathrm{u}, s_{\hat{m}-\zeta+1}) - v(u, s_{\hat{m}-\zeta})] + \lambda_{\Delta s}^{\hat{m}+1}, \tag{3.1}$$

where $l_{\zeta} = (\zeta+1)E_{\zeta+1} - \zeta E_{\zeta}$ and $E_{\zeta} = E_{\psi,2}[-\frac{\psi}{1-\psi}(\zeta\Delta s)^{\psi}]$. It is easy to see that

- $l_{\zeta} > 0$ and $l_0 = E_1, \zeta = 1 : 1 : \hat{m}$,
- $l_0 > l_1 > l_2 > \cdots > l_{\zeta},\ \ l_{\zeta} \to 0$ as $\zeta \to \infty$,
- $\sum\limits_{\zeta=0}^{\hat{m}}(l_{\zeta} - l_{\zeta+1}) + l_{\hat{m}+1} = (E_1 - l_1) + \sum\limits_{\zeta=1}^{\hat{m}-1}(l_{\zeta} - l_{\zeta+1}) + l_{\hat{m}} = E_1$.

Moreover, truncation error $\lambda_{\Delta s}^{\hat{m}+1}$ is given by [49]:

$$\lambda_{\Delta s}^{\hat{m}+1} \le \frac{J(\psi)}{1-\psi}\frac{(\Delta s)^2}{2}\Big[\max_{0\le s\le s_{\hat{m}}}\frac{\partial^2 v(\mathrm{u}, s)}{\partial s^2}\Big]c_1,$$

c_1 is constant, and

$$|\ \lambda_{\Delta s}^{\hat{m}+1}\ | \le \hat{\vartheta}(\Delta s)^2, \tag{3.2}$$

where $\hat{\vartheta}$ is a constant. The nonlinear term in Eq (1.1) can be linearized by the generalized formula used in [50].

$$(v^{\varrho}v_{\mathrm{u}})_j^{\hat{m}+1} = \varrho v_j^{\hat{m}+1}((v)^{\varrho-1}v_{\mathrm{u}})_j^{\hat{m}} + (v_{\mathrm{u}})_j^{\hat{m}+1}(v^{\varrho})_j^{\hat{m}} - \varrho(v^{\varrho}v_{\mathrm{u}})_j^{\hat{m}}, \tag{3.3}$$

where ϱ is a positive integer. Applying the θ-weighted scheme for spatial discretization, forward difference for temporal discretization, and Eq (3.1) for the ABFD to Eq (1.1) yields:

$$\frac{v^{\hat{m}+1}-v^{\hat{m}}}{\Delta s}-\phi\frac{v_{\mathrm{uu}}^{\hat{m}+1}-v_{\mathrm{uu}}^{\hat{m}}}{\Delta s}+\rho^{\psi}\gamma\sum_{\zeta=0}^{\hat{m}}l_{\zeta}[v^{\hat{m}-\zeta+1}-v^{\hat{m}-\zeta}]+\theta(v_{\mathrm{u}}^{\hat{m}+1}+\tau(vv_{\mathrm{u}})^{\hat{m}+1}-\chi v_{\mathrm{uu}}^{\hat{m}+1})$$
$$+(1-\theta)(v_{\mathrm{u}}^{\hat{m}}+\tau(vv_{\mathrm{u}})^{\hat{m}}-\chi v_{\mathrm{uu}}^{\hat{m}})=g(\mathrm{u},s_{\hat{m}+1}),\quad(3.4)$$

where $\gamma=\frac{J(\psi)}{1-\psi}$ and $v^{\hat{m}}=v(\mathrm{u},s_{\hat{m}})$. For $\theta=0$, this is an explicit scheme. When $\theta=0.5$, it becomes the Crank-Nicolson scheme, and for $\theta=1$, it is fully implicit. This problem is solved here for $\theta=1$, which yields better results. Substituting Eq (3.3) into (3.4) and simplifying yields:

$$v^{\hat{m}+1}(1+\tau\Delta s\phi v_{\mathrm{u}}^{\hat{m}}+\rho^{\psi}\Delta s\gamma E_1)+v_{\mathrm{u}}^{\hat{m}+1}(\Delta s\theta+\tau\Delta s\theta v^{\hat{m}})+v_{\mathrm{uu}}^{\hat{m}+1}(-\phi-\chi\theta\Delta s)$$
$$=v^{\hat{m}}(1+\rho^{\psi}\Delta s\gamma E_1)+v_{\mathrm{u}}^{\hat{m}+1}(-(1-\theta)\Delta s+(2\theta-1)\tau\Delta sv^{\hat{m}})+v_{\mathrm{uu}}^{\hat{m}}(-\phi+\chi(1-\theta)\Delta s)$$
$$-\rho^{\psi}\gamma\Delta s\Big(\sum_{\zeta=1}^{\hat{m}}l_{\zeta}(v^{\hat{m}-\zeta+1}-v^{\hat{m}-\zeta})\Big)+\Delta sg(\mathrm{u},s_{\hat{m}+1}).\quad(3.5)$$

Combining Eqs (2.2) and (3.5) with the data in Table 1 results in the following system of equations:

$$y_{j-1}^{\hat{m}+1}(\kappa_0)+y_j^{\hat{m}+1}(\kappa_1)+y_{j+1}^{\hat{m}+1}(\kappa_2)=y_{j-1}^{\hat{m}}(\varpi_1)+y_j^{\hat{m}}(\varpi_2)+y_{j+1}^{\hat{m}}(\varpi_3)$$
$$+\rho^{\psi}\gamma E_1\Big(y_{j-1}^{\hat{m}}(\frac{1}{6})+y_j^{\hat{m}}(\frac{4}{6})+y_{j+1}^{\hat{m}}(\frac{1}{6})\Big)-\rho^{\psi}\gamma\Big[\sum_{\zeta=1}^{\hat{m}}l_{\zeta}\Big((y_{j-1}^{\hat{m}-\zeta+1}-y_{j-1}^{\hat{m}-\zeta})+4(y_j^{\hat{m}-\zeta+1}-y_j^{\hat{m}-\zeta})$$
$$+(y_{j+1}^{\hat{m}-\zeta+1}-y_{j+1}^{\hat{m}-\zeta}))/6\Big]+g(\mathrm{u},s_{\hat{m}+1}),\quad(3.6)$$

where,

$$\kappa_0=\frac{1}{6\Delta s}+\frac{\tau\theta R_1}{12h}+\frac{\rho^{\psi}\gamma E_1}{6}-\frac{\theta}{2h}-\frac{\tau\theta R_2}{12h}-\frac{\phi}{h^2\Delta s}-\frac{\chi\theta}{h^2},$$
$$\kappa_1=\frac{4}{6\Delta s}+\frac{\tau\theta R_1}{3h}+\frac{4\rho^{\psi}\gamma E_1}{6}+\frac{2\phi}{h^2\Delta s}+\frac{2\chi\theta}{h^2},$$
$$\kappa_2=\frac{1}{6\Delta s}+\frac{\tau\theta R_1}{12h}+\frac{\rho^{\psi}\gamma E_1}{6}+\frac{\theta}{2h}+\frac{\tau\theta R_2}{12h}-\frac{\phi}{h^2\Delta s}-\frac{\chi\theta}{h^2},$$
$$\varpi_1=\frac{1}{6\Delta s}+\frac{(1-\theta)}{2h}-\frac{\tau(2\theta-1)R_2}{12h}-\frac{\phi}{h^2\Delta s}+\frac{\chi(1-\theta)}{h^2},$$
$$\varpi_2=\frac{4}{6\Delta s}+\frac{2\phi}{h^2\Delta s}-\frac{2\chi(1-\theta)}{h^2},$$
$$\varpi_3=\frac{1}{6\Delta s}-\frac{(1-\theta)}{2h}+\frac{\tau(2\theta-1)R_2}{12h}-\frac{\phi}{h^2\Delta s}+\frac{\chi(1-\theta)}{h^2},$$
$$R_1=y_{j+1}^{\hat{m}}-y_{j-1}^{\hat{m}},$$
$$R_2=y_{j-1}^{\hat{m}}+4y_j^{\hat{m}}+y_{j+1}^{\hat{m}}.$$

The summation term from the right side of Eq (3.6) is dropped for $\zeta=0$, and this equation is considered for the iteration process for $\zeta\geq 1$. Here, a system of $\hat{N}+1$ linear equations can be obtained for $\hat{N}+3$

unknown parameters $(y_{-1}, y_0, y_1, y_2, y_3, \cdots, y_{\hat{N}+1})^T$. To get $\hat{N}+3$ equations, boundary conditions will be used. Boundary conditions are

$$\begin{cases} (y_{-1}^{\hat{m}+1} + 4y_0^{\hat{m}+1} + y_1^{\hat{m}+1})/6 = f_1^{\hat{m}+1}, \\ (y_{\hat{N}-1}^{\hat{m}+1} + 4y_{\hat{N}}^{\hat{m}+1} + y_{\hat{N}+1}^{\hat{m}+1})/6 = f_2^{\hat{m}+1}. \end{cases} \tag{3.7}$$

Equation (3.6) in matrix form can be written as:

$$CY^{\hat{m}+1} = ZY^{\hat{m}} + R\Big(\sum_{\zeta=0}^{\hat{m}-1}(l_\zeta - l_{\zeta+1})Y^{\hat{m}-\zeta} + l_{\hat{m}}Y^0\Big) + B^{\hat{m}+1}, \tag{3.8}$$

where

$$Y^{\hat{m}+1} = (y_{-1}^{\hat{m}+1}, y_0^{\hat{m}+1}, y_1^{\hat{m}+1}, \cdots, y_{\hat{N}-1}^{\hat{m}+1}, y_{\hat{N}}^{\hat{m}+1}, y_{\hat{N}+1}^{\hat{m}+1})^T,$$

$$C = \begin{pmatrix} \frac{1}{6} & \frac{4}{6} & \frac{1}{6} & 0 & \cdots & 0 & 0 & 0 \\ \kappa_0^{\hat{m}+1} & \kappa_1^{\hat{m}+1} & \kappa_2^{\hat{m}+1} & 0 & \cdots & 0 & 0 & 0 \\ \vdots & \vdots & \vdots & \vdots & \ddots & \vdots & \vdots & \vdots \\ 0 & 0 & 0 & 0 & \cdots & \kappa_0^{\hat{m}+1} & \kappa_1^{\hat{m}+1} & \kappa_2^{\hat{m}+1} \\ 0 & 0 & 0 & 0 & \cdots & \frac{1}{6} & \frac{4}{6} & \frac{1}{6} \end{pmatrix},$$

$$Z = \begin{pmatrix} 0 & 0 & 0 & 0 & \cdots & 0 & 0 & 0 \\ \varpi_1^{\hat{m}} & \varpi_2^{\hat{m}} & \varpi_3^{\hat{m}} & 0 & \cdots & 0 & 0 & 0 \\ \vdots & \vdots & \vdots & \vdots & \ddots & \vdots & \vdots & \vdots \\ 0 & 0 & 0 & 0 & \cdots & \varpi_1^{\hat{m}} & \varpi_2^{\hat{m}} & \varpi_3^{\hat{m}} \\ 0 & 0 & 0 & 0 & \cdots & 0 & 0 & 0 \end{pmatrix}, R = \begin{pmatrix} 0 & 0 & 0 & 0 & \cdots & 0 & 0 & 0 \\ \frac{1}{6} & \frac{4}{6} & \frac{1}{6} & 0 & \cdots & 0 & 0 & 0 \\ \vdots & \vdots & \vdots & \vdots & \ddots & \vdots & \vdots & \vdots \\ 0 & 0 & 0 & 0 & \cdots & \frac{1}{6} & \frac{4}{6} & \frac{1}{6} \\ 0 & 0 & 0 & 0 & \cdots & 0 & 0 & 0 \end{pmatrix} B = \begin{pmatrix} f_1^{\hat{m}+1} \\ g_0^{\hat{m}+1} \\ \vdots \\ g_{\hat{N}}^{\hat{m}+1} \\ f_2^{\hat{m}+1} \end{pmatrix}.$$

Insert the vector $Y^{\hat{m}+1}$ in (2.2), and the numerical solution at $(\hat{m}+1)^{th}$ time stage can be obtained for $\hat{m} = 0, 1, \cdots, \hat{M}$.

4. Initial vector

By using the IC, the initial vector $Y^0 = (y_{-1}^0, y_0^0, y_1^0, ..., y_{\hat{N}-1}^0, y_{\hat{N}}^0, y_{\hat{N}+1}^0)^T$ of the given problem can be calculated. Derivatives are approximated at boundary points and the IC is used to know the value of Y^0 as:

$$(v_{\mathrm{u}})_j^0 = v_0'(\mathrm{u}_j) \text{ for } j = 0 \text{ and } \hat{N},$$
$$(v_{\mathrm{u}})_j^0 = v_0(\mathrm{u}_j) \text{ for } j = 0, 1, 2, \cdots, \hat{N}.$$

This system gives a matrix of dimension $(\hat{N}+3) \times (\hat{N}+3)$,

$$PY^0 = Z_0,$$

where,

$$P = \begin{pmatrix} \frac{-1}{2h} & 0 & \frac{1}{2h} & 0 & \cdots & 0 & 0 & 0 \\ \frac{1}{6} & \frac{4}{6} & \frac{1}{6} & 0 & \cdots & 0 & 0 & 0 \\ \vdots & \vdots & \vdots & \vdots & \ddots & \vdots & \vdots & \vdots \\ 0 & 0 & 0 & 0 & \cdots & \frac{1}{6} & \frac{4}{6} & \frac{1}{6} \\ 0 & 0 & 0 & 0 & \cdots & \frac{-1}{2h} & 0 & \frac{1}{2h} \end{pmatrix}, \; Y^0 = \begin{pmatrix} y_{-1}^0 \\ y_0^0 \\ \vdots \\ y_{\hat{N}}^0 \\ y_{\hat{N}+1}^0 \end{pmatrix}, \text{ and } Z_0 = \begin{pmatrix} v_0'(\mathrm{u}_0) \\ v_0(\mathrm{u}_0) \\ \vdots \\ v_0(\mathrm{u}_{\hat{N}}) \\ v_0'(\mathrm{u}_{\hat{N}}) \end{pmatrix}.$$

5. The stability analysis

The von Neumann stability analysis is based on the decomposition of numerical errors of numerical approximations into Fourier series [51]. This is employed in this section to examine the stability of the proposed numerical scheme. For this, suppose $y_j^{\hat{m}}$ symbolizes the growth factor in Fourier mode as:

$$y_j^{\hat{m}} = \acute{A}\xi^{\hat{m}} exp(ij\mu), \tag{5.1}$$

where $\mu = \mathfrak{p}h$, $\acute{A}$ is the harmonic amplitude, and $\mathfrak{p}$ is the mode number. Now using Eq (5.1) in Eq (3.6), the result is

$$\begin{aligned}(\kappa_0)(\acute{A}\xi^{\hat{m}+1}e^{i(j-1)\mu}) + (\kappa_1)(\acute{A}\xi^{\hat{m}+1}e^{i(j)\mu}) + (\kappa_2)(\acute{A}\xi^{\hat{m}+1}e^{i(j+1)\mu}) = (\varpi_1)(\acute{A}\xi^{\hat{m}}e^{i(j-1)\mu})\\ + (\varpi_2)(\acute{A}\xi^{\hat{m}}e^{i(j)\mu}) + (\varpi_3)(\acute{A}\xi^{\hat{m}}e^{i(j+1)\mu}) - \rho^{\psi}\gamma\Big[\sum_{\zeta=1}^{\hat{m}} l_{\zeta}((\acute{A}\xi^{\hat{m}-\zeta+1}e^{i(j-1)\mu} - \acute{A}\xi^{\hat{m}-\zeta}e^{i(j-1)\mu})\\ + 4(\acute{A}\xi^{\hat{m}-\zeta+1}e^{i(j)\mu} - \acute{A}\xi^{\hat{m}-\zeta}e^{i(j)\mu}) + (\acute{A}\xi^{\hat{m}-\zeta+1}e^{i(j+1)\mu} - \acute{A}\xi^{\hat{m}-\zeta}e^{i(j+1)\mu})/6)\Big] + g(\mathfrak{u}, s_{\hat{m}+1}).\end{aligned} \tag{5.2}$$

After further simplification, Eq (5.2) becomes

$$\begin{aligned}\xi^{\hat{m}+1}[e^{-i\mu}\kappa_0 + \kappa_1 + e^{i\mu}\kappa_2] = \xi^{\hat{m}}[e^{-i\mu}\varpi_1 + \varpi_2 + e^{i\mu}\varpi_3] + (\acute{A})^{-1}e^{-ij\mu}f(\mathfrak{u}, s_{\hat{m}+1}) - \rho^{\psi}\gamma\\ \Big[\sum_{\zeta=0}^{\hat{m}} l_{\zeta}((\xi^{\hat{m}-\zeta+1}e^{-i\mu} - \xi^{\hat{m}-\zeta}e^{-i\mu}) + 4(\xi^{\hat{m}-\zeta+1} - \xi^{\hat{m}-\zeta}) + (\xi^{\hat{m}-\zeta+1}e^{i\mu} - \xi^{\hat{m}-\zeta}e^{i\mu})/6)\Big].\end{aligned} \tag{5.3}$$

Using the values of $\kappa_0,\ \kappa_1,\ \kappa_2,\ \varpi_1,\ \varpi_2$, and ϖ_3 in Eq (5.3), we have

$$\begin{aligned}\xi^{\hat{m}+1} = \xi^{\hat{m}}\frac{\varpi_4 2cos\mu + \varpi_5 2isin\mu + \varpi_2}{[2\kappa_4 cos\mu + \kappa_5 2isin\mu + \kappa_1]}\\ + \frac{A^{-1}e^{-ij\mu}f(\mathfrak{u}, s_{\hat{m}+1}) - \rho^{\psi}\gamma\sum\limits_{\zeta=0}^{\hat{m}} l_{\zeta}[((\xi^{\hat{m}-\zeta+1} - \xi^{\hat{m}-\zeta})(2 + cos\mu))/3]}{[2\kappa_4 cos\mu + \kappa_5 2isin\mu + \kappa_1]},\end{aligned} \tag{5.4}$$

where

$$\begin{aligned}\kappa_4 =& \frac{1}{6\Delta s} + \frac{\tau\theta R_1}{12h} + \frac{\rho^{\psi}\gamma E_1}{6} - \frac{\phi}{h^2\Delta s} - \frac{\chi\theta}{h^2},\\ \kappa_5 =& \frac{\theta}{2h} + \frac{\tau\theta R_2}{12h},\\ \varpi_4 =& \frac{1}{6\Delta s} + \frac{\rho^{\psi}\gamma E_1}{6} - \frac{\phi}{h^2\Delta s} + \frac{\chi(1-\theta)}{h^2},\\ \varpi_5 =& \frac{2\theta - 1}{12h} - \frac{1-\theta}{12h}.\end{aligned}$$

Denominator value is greater than the numerator value. Thus, $|\xi|^2 \leq 1$.

Since the modulus of the eigenvalues must be less than one, the suggested approach for the time-fractional BBM-Burger equation is, therefore, unconditionally stable from (5.4). This indicates that the grid size h and step size Δs in the time level are not limited; rather, we should favor the values of h and Δs that yield the highest scheme accuracy.

6. The convergence analysis

The convergence of the proposed technique is examined using the approach presented in [52]. We first introduce Theorem 1 and Lemma 6.1, which are based on the work of Hall [53] and Boor [54].

Theorem 1. *Assume that* $g(\mathfrak{u}, s)$ *and* $v(\mathfrak{u}, s)$ *belong to* $C^2(\mathfrak{a}, \mathfrak{b})$ *and* $C^4(\mathfrak{a}, \mathfrak{b})$ *respectively. The equidistance partition of* $[\mathfrak{a}, \mathfrak{b}]$ *is* $\Upsilon = [\mathfrak{a} = \mathfrak{u}_0, \mathfrak{u}_1, \mathfrak{u}_2, \cdots, \mathfrak{u}_{\hat{N}} = \mathfrak{b}]$ *with stepsize h. If* $\hat{\Psi}$ *is the unique spline interpolation of the given problem at knots* $\mathfrak{u}_0, \mathfrak{u}_1, \mathfrak{u}_2, \cdots, \mathfrak{u}_{\hat{N}} \in \Upsilon$*, then there exists a constant* $\mathfrak{I}_j$ *independent of h in which* $\mathfrak{u}_j = \mathfrak{a} + jh$*,* $j = 0, 1, 2, \cdots, \hat{N}$*, then for every* $s \geq 0$*, it can be obtained that*

$$\| D^j(v(\mathfrak{u}, s) - \hat{\Psi}(\mathfrak{u}, s)) \| \leq \mathfrak{I}_j h^{4-j}, \quad j = 0, 1, 2. \tag{6.1}$$

Lemma 6.1. *The cubic B-spline set* $F_{-1}, F_0, F_1, \cdots, F_{\hat{N}+1}$ *in Eq (2.3) satisfies the inequality*

$$\sum_{j=-1}^{\hat{N}+1} |F_j(\mathfrak{u})| \leq \frac{5}{3}, \quad 0 \leq \mathfrak{u} \leq 1.$$

Theorem 2. *For the BBM-Burger Eq (1.1) and BCs (1.2), there is a computational approximation* $\Psi(\mathfrak{u}, s)$ *to the analytical solution* $v(\mathfrak{u}, s)$*. Moreover, if* $g \in C^2[\mathfrak{a}, \mathfrak{b}]$*, then*

$$\| v(\mathfrak{u}, s) - \Psi(\mathfrak{u}, s) \|_\infty \leq \tilde{\mathfrak{I}} h^2, \quad \forall \ \ s \geq 0,$$

where h is relatively small and $\tilde{\mathfrak{I}} > 0$ *is free of h.*

Proof. Assume $\Psi(\mathfrak{u}, s)$ is approximated as $\hat{\Psi}(\mathfrak{u}, s) = \sum_{j=-1}^{\hat{N}+1} w_j^{\hat{m}}(t) F_j(\mathfrak{u})$. From triangular inequality:

$$\| v(\mathfrak{u}, s) - \Psi(\mathfrak{u}, s) \|_\infty \leq \| v(\mathfrak{u}, s) - \hat{\Psi}(\mathfrak{u}, s) \|_\infty + \| \hat{\Psi}(\mathfrak{u}, s) - \Psi(\mathfrak{u}, s) \|_\infty . \tag{6.2}$$

By using Theorem 1, Eq (6.2) becomes:

$$\| v(\mathfrak{u}, s) - \Psi(\mathfrak{u}, s) \|_\infty \leq \mathfrak{I}_0 h^4 + \| \hat{\Psi}(\mathfrak{u}, s) - \Psi(\mathfrak{u}, s) \|_\infty . \tag{6.3}$$

The proposed scheme has collocation conditions as: $Lv(\mathfrak{u}_j, s) = L\Psi(\mathfrak{u}_j, s) = g(\mathfrak{u}_j, s), \quad j = 0(1)\hat{N}$. Suppose that $L\hat{\Psi}(\mathfrak{u}_j, s) = \hat{g}(\mathfrak{u}_j, s)$, $j = 0(1)\hat{N}$. Thus, for any temporal level, the difference $\hat{\Psi}(\mathfrak{u}_j, s) - \Psi(\mathfrak{u}_j, s)$ with $\theta = 1$ in linear form can be given as:

$$\begin{aligned}
\Omega_{j-1}^{\hat{m}+1}(\kappa_6) + \Omega_j^{\hat{m}+1}(\kappa_7) + \Omega_{j+1}^{\hat{m}+1}(\kappa_8) = {} & \left(\frac{1}{6}\Omega_{j-1}^{\hat{m}} + \frac{4}{6}\Omega_j^{\hat{m}} + \frac{1}{6}\Omega_{j+1}^{\hat{m}}\right) - \phi\left(\frac{1}{h^2}\Omega_{j-1}^{\hat{m}} - \frac{2}{h^2}\Omega_j^{\hat{m}} + \frac{1}{h^2}\Omega_{j+1}^{\hat{m}}\right) \\
& + \rho^\psi \Delta s \gamma l_0 \left(\frac{1}{6}\Omega_{j-1}^{\hat{m}} + \frac{4}{6}\Omega_j^{\hat{m}} + \frac{1}{6}\Omega_{j+1}^{\hat{m}}\right) - \rho^\psi \Delta s \gamma \Big[\sum_{\zeta=1}^{\hat{m}} l_\zeta ((\Omega_{j-1}^{\hat{m}-\zeta+1} - \Omega_{j-1}^{\hat{m}-\zeta}) + 4(\Omega_j^{\hat{m}-\zeta+1} - \Omega_j^{\hat{m}-\zeta}) \\
& + (\Omega_{j+1}^{\hat{m}-\zeta+1} - \Omega_{j+1}^{\hat{m}-\zeta}))/6 \Big] + \Delta s \frac{\beta_j^{\hat{m}+1}}{h^2},
\end{aligned} \tag{6.4}$$

where

$$\kappa_6 = \frac{1}{6} - \frac{\phi}{h^2} - \frac{\Delta s \tau \psi}{2h} - \frac{\Delta s \chi}{h^2} - \frac{\Delta s}{2h} + \frac{\rho^\psi \Delta s E_1 \gamma}{6},$$

$$\kappa_7 = \frac{4}{6} + \frac{2\phi}{h^2} + \frac{2\Delta s\chi}{h^2} + \frac{4\rho^{\psi}\Delta sE_1\gamma}{6},$$
$$\kappa_8 = \frac{1}{6} - \frac{\phi}{h^2} + \frac{\Delta s\tau\psi}{2h} - \frac{\Delta s\chi}{h^2} + \frac{\Delta s}{2h} + \frac{\rho^{\psi}\Delta sE_1\gamma}{6}.$$

BCs can be written as:

$$\frac{1}{6}\Omega_{j-1}^{\hat{m}+1} + \frac{4}{6}\Omega_j^{\hat{m}+1} + \frac{1}{6}\Omega_{j+1}^{\hat{m}+1} = 0, \quad j = 0, \hat{N},$$

where

$$\Omega_j^{\hat{m}} = y_j^{\hat{m}} - w_j^{\hat{m}}, \quad j = -1 : 0 : \hat{N} + 1,$$

and

$$\beta_j^{\hat{m}} = h^2[g_j^{\hat{m}} - \tilde{g}_j^{\hat{m}}], \quad j = 0 : 1 : \hat{N}.$$

From inequality (6.1), it is clear that

$$| \beta_j^{\hat{m}} |= h^2 \mid g_j^{\hat{m}} - \tilde{g}_j^{\hat{m}} |\leq \Im h^4.$$

Define $\beta^{\hat{m}} = max\{| \beta_j^{\hat{m}} |; 0 \leq j \leq \hat{N}\}$, $e_j^{\hat{m}} =| \Omega_j^{\hat{m}} |$ and $e^{\hat{m}} = max\{| e_j^{\hat{m}} |; 0 \leq j \leq \hat{N}\}$. When $\hat{m} = 0$, Eq (6.4) becomes

$$\Omega_{j-1}^1(\kappa_6) + \Omega_j^1(\kappa_7) + \Omega_{j+1}^1(\kappa_8) = \left(\frac{1}{6}\Omega_{j-1}^0 + \frac{4}{6}\Omega_j^0 + \frac{1}{6}\Omega_{j+1}^0\right) - \phi\left(\frac{1}{h^2}\Omega_{j-1}^0 - \frac{2}{h^2}\Omega_j^0 + \frac{1}{h^2}\Omega_{j+1}^0\right)$$
$$+ \rho^{\psi}\Delta s\gamma l_0\left(\frac{1}{6}\Omega_{j-1}^0 + \frac{4}{6}\Omega_j^0 + \frac{1}{6}\Omega_{j+1}^0\right) + \Delta s\frac{\beta_j^1}{h^2}. \quad (6.5)$$

From IC, $e^0 = 0$. For sufficiently small mesh spacing h and norms of β_i^1, Ω_i^1, Eq (6.5) yields:

$$e_j^1 \leq \frac{3\Delta s\Im h^4}{h^2 + 12\phi + 12\Delta s\chi + h^2\Delta s\rho^{\psi}\gamma E_1}.$$

From BCs e_{-1}^1 and $e_{\hat{N}+1}^1$, it can be written as:

$$e_{-1}^1 \leq \frac{15\Delta s\Im h^4}{h^2 + 12\phi + 12\Delta s\chi + h^2\Delta s\rho^{\psi}\gamma E_1},$$

$$e_{\hat{N}+1}^1 \leq \frac{15\Delta s\Im h^4}{h^2 + 12\phi + 12\Delta s\chi + h^2\Delta s\rho^{\psi}\gamma E_1}.$$

From above conditions, it is carried out that

$$e^1 \leq \Im_1 h^2,$$

where $\Im_1$ is not depending on h. To prove this theorem, mathematical induction is applied to $\hat{m}$. It is considered that the term $e_j^z \leq \Im_z h^2$ is true, when $z = 1, 2, 3, \cdots, \hat{m}$ and $\Im = max\{\Im_z : z = 0, 1, 2, \cdots, \hat{m}\}$, then Eq (6.4) becomes:

$$\Omega_{j-1}^{\hat{m}+1}(\kappa_6)+\Omega_{j}^{\hat{m}+1}(\kappa_7)+\Omega_{j+1}^{\hat{m}+1}(\kappa_8)=\left(\frac{1}{6}\Omega_{j-1}^{\hat{m}}+\frac{4}{6}\Omega_{j}^{\hat{m}}+\frac{1}{6}\Omega_{j+1}^{\hat{m}}\right)-\phi\left(\frac{1}{h^2}\Omega_{j-1}^{\hat{m}}-\frac{2}{h^2}\Omega_{j}^{\hat{m}}+\frac{1}{h^2}\Omega_{j+1}^{\hat{m}}\right)$$
$$+\rho^{\psi}\Delta s\gamma(l_0-l_1)\left(\frac{1}{6}\Omega_{j-1}^{\hat{m}}+\frac{4}{6}\Omega_{j}^{\hat{m}}+\frac{1}{6}\Omega_{j+1}^{\hat{m}}\right)+\rho^{\psi}\Delta s\gamma(l_1-l_2)\left(\frac{1}{6}\Omega_{j-1}^{\hat{m}-1}+\frac{4}{6}\Omega_{j}^{\hat{m}-1}+\frac{1}{6}\Omega_{j+1}^{\hat{m}-1}\right)$$
$$+\rho^{\psi}\Delta s\gamma(l_2-l_3)\left(\frac{1}{6}\Omega_{j-1}^{\hat{m}-2}+\frac{4}{6}\Omega_{j}^{\hat{m}-2}+\frac{1}{6}\Omega_{j+1}^{\hat{m}-2}\right)+\cdots+\rho^{\psi}\Delta s\gamma(l_{\hat{m}-2}-l_{\hat{m}-1})\left(\frac{1}{6}\Omega_{j-1}^{2}+\frac{4}{6}\Omega_{j}^{2}+\frac{1}{6}\Omega_{j+1}^{2}\right)$$
$$+\rho^{\psi}\Delta s\gamma(l_{\hat{m}-1}-l_{\hat{m}})\left(\frac{1}{6}\Omega_{j-1}^{1}+\frac{4}{6}\Omega_{j}^{1}+\frac{1}{6}\Omega_{j+1}^{1}\right)+\rho^{\psi}\Delta s\gamma l_{\hat{m}}\left(\frac{1}{6}\Omega_{j-1}^{0}+\frac{4}{6}\Omega_{j}^{0}+\frac{1}{6}\Omega_{j+1}^{0}\right)+\Delta s\frac{\beta_j^{\hat{m}+1}}{h^2}. \quad (6.6)$$

Apply the norm again on $\Omega_j^{\hat{m}+1}$ and $\beta_j^{\hat{m}+1}$, and Eq (6.6) gives

$$e_j^{\hat{m}+1}\leq\frac{3\Im h^4}{(h^2+12\phi+12\Delta s\chi+h^2\Delta s\rho^{\psi}\gamma E_1)}\left(1+\Delta s+\Delta s\rho^{\psi}\gamma\sum_{\zeta=0}^{\hat{m}-1}(l_\zeta-l_{\zeta+1})\right).$$

Similarly, from BCs $e_{-1}^{\hat{m+1}}$ and $e_{\hat{N}+1}^{\hat{m}+1}$, it can be taken as:

$$e_{-1}^{\hat{m}+1}\leq\frac{15\Im h^4}{(h^2+12\phi+12\Delta s\chi+h^2\Delta s\rho^{\psi}\gamma E_1)}\left(1+\Delta s+\Delta s\rho^{\psi}\gamma\sum_{\zeta=0}^{\hat{m}-1}(l_\zeta-l_{\zeta+1})\right),$$

$$e_{\hat{N}+1}^{\hat{m}+1}\leq\frac{15\Im h^4}{(h^2+12\phi+12\Delta s\chi+h^2\Delta s\rho^{\psi}\gamma E_1)}\left(1+\Delta s+\Delta s\rho^{\psi}\gamma\sum_{\zeta=0}^{\hat{m}-1}(l_\zeta-l_{\zeta+1})\right).$$

For all $\hat{m}$, we get

$$e^{\hat{m}+1}\leq\Im h^2. \quad (6.7)$$

Particularly,

$$\hat{\Psi}(\mathfrak{u},s)-\Psi(\mathfrak{u},s)=\sum_{j=-1}^{\hat{N}+1}(w_j(s)-y_j(s))F_j(\mathfrak{u}).$$

Therefore, the inequality (6.7) and Lemma 6.1 gives

$$\|\hat{\Psi}(\mathfrak{u},s)-\Psi(\mathfrak{u},s)\|_{\infty}\leq\frac{5}{3}\Im h^2. \quad (6.8)$$

From inequalities (6.3) and (6.8), we obtain:

$$\|v(\mathfrak{u},s)-\Psi(\mathfrak{u},s)\|_{\infty}\leq\Im_0 h^4+\frac{5}{3}\Im h^2=\check{\Im}h^2,$$

where $\check{\Im}=\Im_0 h^2+\frac{5}{3}\Im$. □

Theorem 3. *The BBM-Burger equation is convergent with the initial and BCs.*

Proof. Consider the BBM-Burger equation has analytical solution $v(\mathfrak{u},s)$ and numerical solution $\Psi(\mathfrak{u},s)$. Therefore, the previous theorem and inequality (3.2) validate that

$$\|v(\mathfrak{u},s)-\Psi(\mathfrak{u},s)\|_{\infty}\leq\check{\Im}h^2+\hat{\vartheta}(\Delta s)^2, \quad (6.9)$$

where $\check{\Im}$ and $\hat{\vartheta}$ are arbitrary constants. Consequently, the present scheme is second order convergent in both the spatial and temporal directions. □

7. Examples and discussion

This section includes numerical results and their consistency to show how accurate our results are. Error norms $L_2(\hat{N})$ and $L_\infty(\hat{N})$ are defined as:

$$L_2(\hat{N}) = \|v(\mathrm{u}_j, s) - \Psi(\mathrm{u}_j, s)\|_2 = \sqrt{h \sum_{j=0}^{\hat{N}} \mid v(\mathrm{u}_j, s) - \Psi(\mathrm{u}_j, s) \mid^2},$$
$$L_\infty(\hat{N}) = \|v(\mathrm{u}_j, s) - \Psi(\mathrm{u}_j, s)\|_\infty = \max_{0 \le j \le \hat{N}} \mid v(\mathrm{u}_j, s) - \Psi(\mathrm{u}_j, s) \mid .$$

The convergence order of the present scheme can be calculated as [55]:

$$log\Big(\frac{L_\infty(\hat{N})}{L_\infty(\hat{N}+1)}\Big) \diagup log\Big(\frac{(\hat{N}+1)}{(\hat{N})}\Big).$$

Normalization function in all examples is considered as $R(\psi) = 1$ and $\theta = 1$. Mathematica 9 is used for numerical calculations on an Intel(R)Core(TM) i5-3437U CPU@2.60GHz, 2712Mhz with 16GB RAM, SSD and 64-bit operating system (Windows 11 pro). Processing to compute numerical results takes less than a minute for all computed results given in tables.

Example 7.1. *Consider the nonhomogeneous time-fractional BBM-Burger Eq (1.1) with specific parameter values, namely,* $\phi = \rho = \tau = \chi = 1$.

$$v_s + v_{\mathrm{u}} - v_{\mathrm{uus}} + \rho^\psi D_s^\psi v + v v_{\mathrm{u}} - v_{\mathrm{uu}} = g(\mathrm{u}, s), \qquad s \in [0, S],\ \mathrm{u} \in [0, 2],\ 0 < \psi \le 1,$$

with IC and BCs

$$\begin{cases} v(\mathrm{u}, 0) = 0, \\ v(0, s) = s^2,\ v(2, s) = s^2 e^2, \end{cases}$$

and the source term is $g(\mathrm{u}, s) = 2\Big(\frac{R(\psi)}{1-\psi}\Big) s^2 e^{\mathrm{u}} E_{\psi,3}\Big[\frac{-\psi}{1-\psi} s^\psi\Big] + s^4 e^{2\mathrm{u}}$.

The exact solution is $v(\mathrm{u}, s) = s^2 e^{\mathrm{u}}$. Tables 2 and 3 compare exact and computational solutions, along with absolute errors, for different choices of ψ and $s = 0.25, 0.75$, $\psi = 0.5$ with $\hat{N} = 80$ and $\hat{N} = 60$, $\Delta s = 0.001$, respectively, demonstrating good agreement between the exact and approximate solutions. Error norms for various ψ values are displayed in Table 4 at different time stages. The comparison of error norms and the convergence order for different choices of Δs is represented in Table 5. Table 6 illustrates convergence order and error norm for different values of h. A very good agreement between exact and spline solutions at various time levels for fixed $\hat{N} = 40$ with $\psi = 0.3$ and $\Delta s = 0.01$ is shown in Figure 1. This figure also demonstrates good results for $\hat{N} = 80$, $\psi = 0.7$, and $\Delta s = 0.002$. The correctness of the suggested approach is demonstrated in Figure 2 using 3D graphs comparing analytical and numerical answers at $\hat{N} = 60$, $\psi = 0.5$, $\Delta s = 0.001$, and $s = 1$. At $s = 1$, 2D and 3D error profiles are demonstrated in Figure 3. All tables and figures guarantee the exactness of the scheme.

Table 2. Absolute error for different choices of ψ with $\hat{N} = 80$, $s = 1$, and $\Delta s = 0.001$ of Example 7.1.

		Approximate Solution		Absolute Error	
u	Exact Solution	$\psi = 0.2$	$\psi = 0.7$	$\psi = 0.2$	$\psi = 0.7$
0.0	1	0.999999999999	0.999999999999	3.78141×10^{-13}	5.09814×10^{-13}
0.2	1.221402758160	1.221392348771	1.221392808075	1.04093×10^{-5}	9.95008×10^{-6}
0.4	1.491824697641	1.491804802626	1.491805721466	1.98950×10^{-5}	1.89761×10^{-5}
0.6	1.822118800390	1.822090386954	1.822091728899	2.84134×10^{-5}	2.70714×10^{-5}
0.8	2.225540928492	2.225505139956	2.225506833758	3.57885×10^{-5}	3.40947×10^{-5}
1.0	2.718281828459	2.718240173922	2.718242113097	4.16545×10^{-5}	3.97153×10^{-5}
1.2	3.320116922736	3.320071566803	3.320073606814	4.53559×10^{-5}	4.33159×10^{-5}
1.4	4.055199966844	4.055154197542	4.055156150339	4.57693×10^{-5}	4.38165×10^{-5}
1.6	4.953032424395	4.952991444977	4.952993070875	4.09794×10^{-5}	3.93535×10^{-5}
1.8	6.049647464412	6.049619788339	6.049620786205	2.76760×10^{-5}	2.66782×10^{-5}
2.0	7.389056098930	7.389056098930	7.389056098930	0	0

Table 3. Absolute error norms for different choices of s with $\hat{N} = 60$, $\psi = 0.5$, and $\Delta s = 0.001$ of Example 7.1.

	$s = 0.25$	$s = 0.75$		$s = 0.25$	$s = 0.75$
Exact	Approximate	Exact	Approximate	Absolute Error	Absolute Error
0.0625000000	0.0625000000	0.5625000000	0.5625000000	9.603×10^{-15}	1.479×10^{-13}
0.0763376723	0.0763360796	0.6870390514	0.6870267888	1.592×10^{-6}	1.226×10^{-5}
0.0932390436	0.0932360506	0.8391513924	0.8391280897	2.992×10^{-6}	2.330×10^{-5}
0.1138824250	0.1138782314	1.0249418252	1.0249087651	4.193×10^{-6}	3.306×10^{-5}
0.1390963080	0.1390911427	1.2518667722	1.2518254715	5.165×10^{-6}	4.130×10^{-5}
0.1698926142	0.1698867632	1.5290335285	1.5289859675	5.851×10^{-6}	4.756×10^{-5}
0.2075073076	0.2075011476	1.8675657690	1.8675147100	6.160×10^{-6}	5.105×10^{-5}
0.2534499979	0.2534440400	2.2810499813	2.2809994257	5.957×10^{-6}	5.055×10^{-5}
0.3095645265	0.3095594719	2.7860807387	2.7860366082	5.054×10^{-6}	4.413×10^{-5}
0.3781029665	0.3780997789	3.4029266987	3.4028978806	3.187×10^{-6}	2.881×10^{-5}
0.4618160061	0.4618160061	4.1563440556	4.1563440556	1.110×10^{-16}	8.881×10^{-16}

Table 4. Error norms for different values of ψ, whereas $\Delta s = 0.002$, and $\hat{N} = 120$ of Example 7.1.

	$L_\infty(\hat{N})$			$L_2(\hat{N})$		
s	$\psi = 0.1$	$\psi = 0.5$	$\psi = 0.9$	$\psi = 0.1$	$\psi = 0.5$	$\psi = 0.9$
0.2	9.94079×10^{-7}	9.81215×10^{-7}	8.84006×10^{-7}	1.01832×10^{-6}	1.00509×10^{-6}	9.05239×10^{-7}
0.4	3.77369×10^{-6}	3.68997×10^{-6}	3.13395×10^{-6}	3.86106×10^{-6}	3.77527×10^{-6}	3.20615×10^{-6}
0.6	7.36909×10^{-6}	7.14659×10^{-6}	5.75676×10^{-6}	7.54395×10^{-6}	7.31676×10^{-6}	5.90012×10^{-6}
0.8	9.65892×10^{-6}	9.27306×10^{-6}	6.84334×10^{-6}	9.91894×10^{-6}	9.52635×10^{-6}	7.04179×10^{-6}
1.0	7.88589×10^{-6}	7.43121×10^{-6}	4.52746×10^{-6}	7.95573×10^{-6}	7.47227×10^{-6}	4.29801×10^{-6}

Table 5. Comparison of error norm with distinct values of $\Delta s = \frac{1}{\hat{M}}$, when $s = 1$, $\hat{N} = 60$, and $h = \frac{2}{\hat{N}}$ for Example 7.1.

ψ	$\hat{M}$	$L_\infty(\hat{N})$	$L_2(\hat{N})$	Order
0.2	10	3.67022×10^{-2}	3.46856×10^{-2}	...
	20	9.42441×10^{-3}	8.9247×10^{-3}	1.96139
	40	2.33138×10^{-3}	2.20614×10^{-3}	2.01522
	80	5.23722×10^{-4}	4.90554×10^{-4}	2.15431
	160	6.85997×10^{-5}	5.80062×10^{-5}	2.93253
0.3	10	3.67142×10^{-2}	3.46928×10^{-2}	...
	20	9.43083×10^{-3}	8.93013×10^{-3}	1.96088
	40	2.33379×10^{-3}	2.2083×10^{-3}	2.01471
	80	5.24667×10^{-4}	4.91436×10^{-4}	2.15327
	160	6.90639×10^{-5}	5.84713×10^{-5}	2.92546
0.4	10	3.67304×10^{-2}	3.47023×10^{-2}	...
	20	9.43919×10^{-3}	8.93661×10^{-3}	1.96024
	40	2.33666×10^{-3}	2.2108×10^{-3}	2.01421
	80	5.25812×10^{-4}	4.92489×10^{-4}	2.15183
	160	6.96661×10^{-5}	5.9075×10^{-5}	2.91602
0.5	10	3.6767×10^{-2}	3.473×10^{-2}	...
	20	9.45364×10^{-3}	8.94847×10^{-3}	1.95947
	40	2.34118×10^{-3}	2.21475×10^{-4}	2.01363
	80	5.27459×10^{-4}	4.94012×10^{-4}	2.15011
	160	7.04993×10^{-5}	5.99106×10^{-5}	2.90338

Table 6. Comparison of error norms with distinct values of h, when $s = 1$, $\Delta s = \frac{1}{\hat{M}}$, and $\hat{N} = 100$ for Example 7.1.

ψ	h	$L_\infty(\hat{N})$	$L_2(\hat{N})$	Order
0.2	$\frac{1}{2}$	2.07143×10^{-2}	2.10695×10^{-2}	...
	$\frac{1}{4}$	4.64235×10^{-3}	4.73467×10^{-3}	2.15776
	$\frac{1}{8}$	8.71729×10^{-4}	8.93474×10^{-4}	2.41294
	$\frac{1}{16}$	1.00684×10^{-4}	7.38965×10^{-5}	3.11404
0.3	$\frac{1}{2}$	2.06423×10^{-2}	2.09873×10^{-2}	...
	$\frac{1}{4}$	4.62263×10^{-3}	4.71485×10^{-3}	2.15882
	$\frac{1}{8}$	8.66622×10^{-4}	8.88302×10^{-4}	2.41524
	$\frac{1}{16}$	1.01944×10^{-4}	7.50392×10^{-5}	3.08763
0.4	$\frac{1}{2}$	2.05389×10^{-2}	2.08701×10^{-2}	...
	$\frac{1}{4}$	4.59445×10^{-3}	4.68654×10^{-3}	2.16043
	$\frac{1}{8}$	8.59434×10^{-4}	8.81023×10^{-4}	2.41843
	$\frac{1}{16}$	1.03629×10^{-4}	7.65899×10^{-5}	3.05196
0.5	$\frac{1}{2}$	2.03979×10^{-2}	2.07107×10^{-2}	...
	$\frac{1}{4}$	4.55611×10^{-3}	4.64804×10^{-3}	2.16255
	$\frac{1}{8}$	8.49624×10^{-4}	8.71091×10^{-4}	2.42291
	$\frac{1}{16}$	1.06076×10^{-4}	7.87782×10^{-5}	3.00173

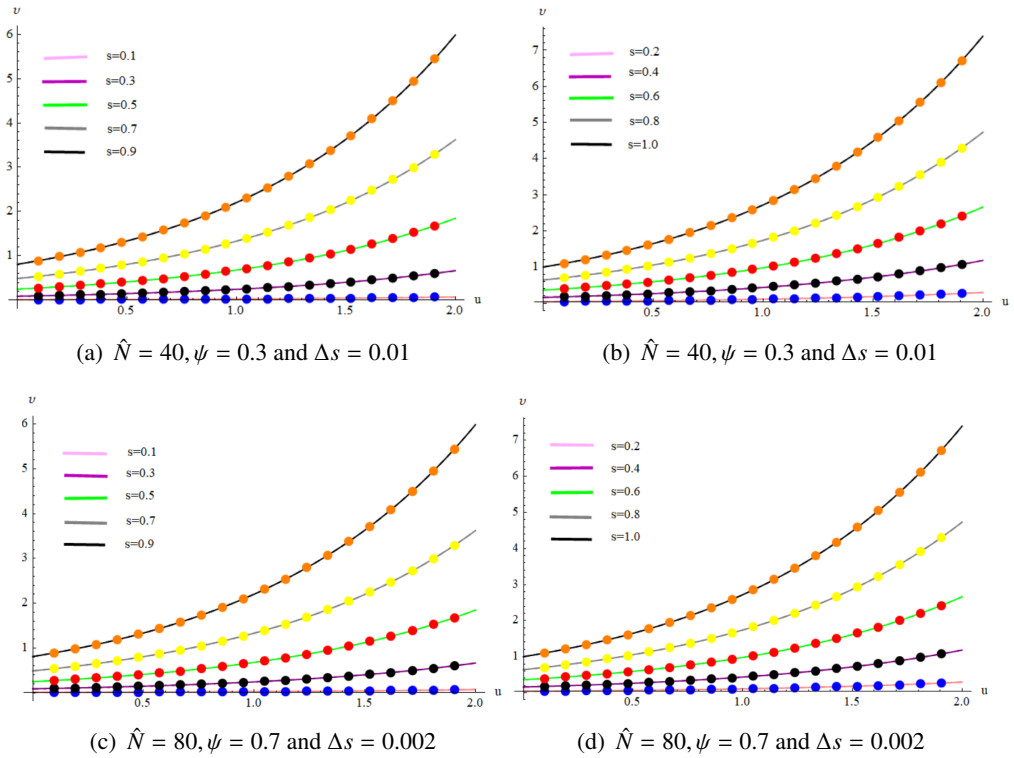

(a) $\hat{N} = 40, \psi = 0.3$ and $\Delta s = 0.01$ (b) $\hat{N} = 40, \psi = 0.3$ and $\Delta s = 0.01$

(c) $\hat{N} = 80, \psi = 0.7$ and $\Delta s = 0.002$ (d) $\hat{N} = 80, \psi = 0.7$ and $\Delta s = 0.002$

Figure 1. Exact and numerical solutions for Example 7.1 at different temporal stages.

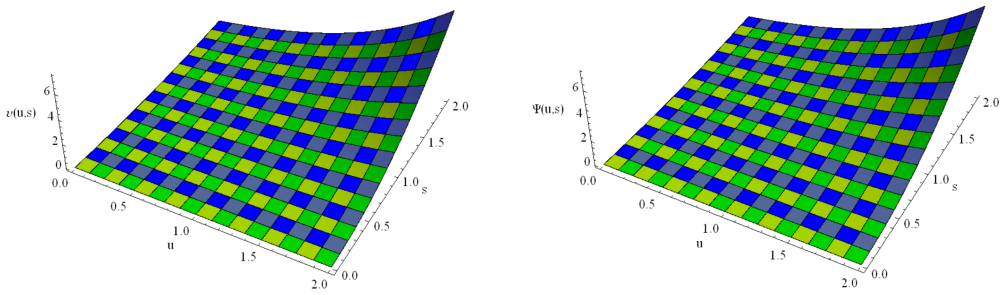

(a) Exact solution, (b) Approximate solution

Figure 2. 3D exact and approximate solution for Example 7.1, when $\hat{N} = 60$, $\psi = 0.5$, $\Delta s = 0.001$, and $s = 1$.

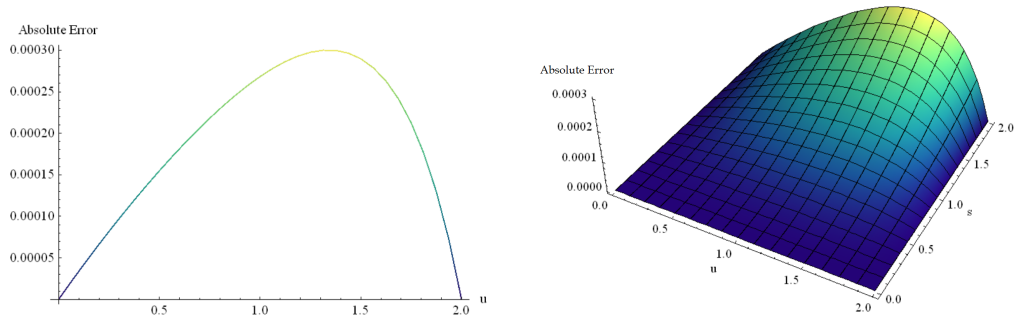

(a) 2D error graph (b) 3D error space-time graph

Figure 3. 2D and 3D error profiles for Example 7.1, when $\hat{N} = 32$, $\psi = 0.6$, $\Delta s = 0.001$, and $s = 1$.

Example 7.2. *Consider the nonhomogeneous time-fractional BBM-Burger Eq (1.1) with specific parameter values, namely,* $\phi = \rho = \tau = \chi = 1$.

$$v_s + v_{\mathrm{u}} - v_{\mathrm{uus}} + \rho^{\psi} D_s^{\psi} v + v v_{\mathrm{u}} - v_{\mathrm{uu}} = g(\mathrm{u}, s), \quad s \in [0, S], \ \mathrm{u} \in [0, 2], \ 0 < \psi \leq 1,$$

with IC and BCs

$$\begin{cases} v(\mathrm{u}, 0) = 0, \\ v(0, s) = 0, \ v(2, s) = s^3 \sin(2), \end{cases}$$

and the source term is $g(\mathrm{u}, s) = 6\left(\frac{R(\psi)}{1-\psi}\right) s^3 \sin(\mathrm{u}) E_{\psi,4}\left[\frac{-\psi}{1-\psi} s^{\psi}\right] + 3s^2 \sin(\mathrm{u}) + s^3 cos(\mathrm{u}) + 3s^2 \sin(\mathrm{u}) + (s^3 \sin(\mathrm{u}))(s^3 \cos(\mathrm{u})) + s^3 \sin(\mathrm{u})$.

The exact solution is $\psi(\mathrm{u}, s) = s^3 sin(\mathrm{u})$. The absolute errors for various values of u setting $\Delta s = 0.001$, $s = 1$, $\psi = 0.5$, and $\hat{N} = 30$ are reported in Table 7 of Example 7.2. Table 8 presents the exact solutions, approximate results, and absolute errors for the proposed problem when $\Delta s = 0.001$, $s = 0.25$, $\psi = 0.2$, $\hat{N} = 50$. Comparison of error norms is tabulated in Table 9. Tables 10 and 11 exhibit error norms and their convergence orders for various choices of parameters in temporal and

spatial directions. Figure 4 shows the significant agreement between the numerical findings and exact solutions of the suggested scheme at different time levels. A 3D representation of exact and computational solutions at distinct values of parameters is given in Figure 5. The 2D and 3D error profile is exhibited in Figure 6, which demonstrates procedure of best accuracy.

Table 7. Absolute error of Example 7.2 with $\Delta s = 0.001$, $s = 1$, $\psi = 0.5$, and $\hat{N} = 30$.

u	Exact solution	Approximate solution	Absolute Error
0.0	0	1.41512×10^{-14}	1.41512×10^{-14}
0.2	0.198669330	0.198782763	0.000113432
0.4	0.389418342	0.389644040	0.000225698
0.6	0.564642473	0.564970890	0.000328417
0.8	0.717356090	0.717768999	0.000412908
1.0	0.841470984	0.841941093	0.000470108
1.2	0.932039085	0.932529613	0.000490527
1.4	0.985449729	0.985913966	0.000464236
1.6	0.999573603	0.999954505	0.000380902
1.8	0.973847630	0.974077462	0.000229831
2.0	0.909297426	0.909297426	0

Table 8. Absolute error of Example 7.2 for $\Delta s = 0.001$, $s = 0.25$, $\psi = 0.2$, and $\hat{N} = 50$.

u	Exact solution	Approximate solution	Absolute Error
0.0	0	-4.99873×10^{-16}	4.99873×10^{-16}
0.2	0.003104208	0.003107163	2.95558×10^{-6}
0.4	0.006084661	0.006090412	5.75135×10^{-6}
0.6	0.008822538	0.008830720	8.18207×10^{-6}
0.8	0.011208688	0.011218739	1.00503×10^{-5}
1.0	0.013147984	0.013159153	1.11693×10^{-5}
1.2	0.014563110	0.014574477	1.13666×10^{-5}
1.4	0.015397652	0.015408136	1.04846×10^{-5}
1.6	0.015618337	0.015626718	8.38092×10^{-6}
1.8	0.015216369	0.015221295	4.92614×10^{-6}
2.0	0.014207772	0.014207772	1.73472×10^{-18}

Table 9. Error norms for distinct values of ψ, where $\hat{N} = 40$, and $\Delta s = 0.001$ of Example 7.2.

	$L_\infty(\hat{N})$			$L_2(\hat{N})$		
s	$\psi = 0.2$	$\psi = 0.5$	$\psi = 0.8$	$\psi = 0.2$	$\psi = 0.5$	$\psi = 0.8$
0.2	5.77880×10^{-6}	5.72266×10^{-6}	5.51977×10^{-6}	5.85582×10^{-6}	5.79904×10^{-6}	5.59391×10^{-6}
0.4	4.30703×10^{-5}	4.24272×10^{-5}	4.03835×10^{-5}	4.35810×10^{-5}	4.29325×10^{-5}	4.08728×10^{-5}
0.6	1.35549×10^{-4}	1.33144×10^{-4}	1.26329×10^{-4}	1.36972×10^{-4}	1.34554×10^{-4}	1.27708×10^{-4}
0.8	2.99387×10^{-4}	2.93729×10^{-4}	2.79364×10^{-4}	3.02142×10^{-4}	2.96474×10^{-4}	2.82029×10^{-4}
1.0	5.44153×10^{-4}	5.34025×10^{-4}	5.10643×10^{-4}	5.47508×10^{-4}	5.37333×10^{-4}	5.13911×10^{-4}

Table 10. Comparison of error norm with distinct values of $\Delta s = \frac{1}{\hat{M}}$, when $s = 1$, $\hat{N} = 10$, and $h = \frac{2}{\hat{N}}$ for Example 7.2.

ψ	$\hat{M}$	$L_\infty(\hat{N})$	$L_2(\hat{N})$	Order
0.2	100	5.10677×10^{-3}	5.13719×10^{-3}	...
	200	2.09648×10^{-3}	2.10751×10^{-3}	1.28444
	400	5.92019×10^{-4}	5.93432×10^{-4}	1.82425
	800	1.59913×10^{-4}	1.63783×10^{-4}	1.88836
0.3	100	5.08562×10^{-3}	5.11596×10^{-3}	...
	200	2.08753×10^{-3}	2.09853×10^{-3}	1.28463
	400	5.89267×10^{-4}	5.90684×10^{-4}	1.82480
	800	1.59537×10^{-4}	1.63384×10^{-4}	1.88503
0.4	100	5.05523×10^{-3}	5.8544×10^{-3}	...
	200	2.07469×10^{-3}	2.08565×10^{-3}	1.28488
	400	5.85347×10^{-4}	5.86771×10^{-4}	1.82553
	800	1.58962×10^{-4}	1.62774×10^{-4}	1.88061
0.5	100	5.01418×10^{-3}	5.04424×10^{-3}	...
	200	2.05742×10^{-3}	2.06834×10^{-3}	1.28518
	400	5.80171×10^{-4}	5.8161×10^{-4}	1.82629
	800	1.58041×10^{-4}	1.61803×10^{-4}	1.87618

Table 11. Comparison of error norm with distinct values of h, when $s = 1$, $h = \frac{2}{\hat{N}}$, $\hat{M} = 1200$ for Example 7.2.

ψ	$\hat{N}$	$L_\infty(\hat{N})$	$L_2(\hat{N})$	Order
0.2	2	2.19161×10^{-2}	2.19161×10^{-2}	...
	4	5.04859×10^{-3}	5.25733×10^{-3}	2.11804
	8	9.17818×10^{-4}	9.33769×10^{-4}	2.45965
	16	1.45032×10^{-4}	1.45084×10^{-4}	2.66184
0.3	2	2.18407×10^{-2}	2.18407×10^{-2}	...
	4	5.02905×10^{-3}	5.23767×10^{-3}	2.11867
	8	9.14482×10^{-4}	9.30322×10^{-4}	2.45926
	16	1.44311×10^{-4}	1.44359×10^{-4}	2.66378
0.4	2	2.17315×10^{-2}	2.17315×10^{-2}	...
	4	5.00074×10^{-3}	5.20919×10^{-3}	2.11957
	8	9.09634×10^{-4}	9.25313×10^{-4}	2.45878
	16	1.43289×10^{-4}	1.43332×10^{-4}	2.66636
0.5	2	2.15801×10^{-2}	2.15801×10^{-2}	...
	4	4.96149×10^{-3}	5.16970×10^{-3}	2.12085
	8	9.02844×10^{-4}	9.18299×10^{-4}	2.45823
	16	1.41956×10^{-4}	1.41997×10^{-4}	2.66903

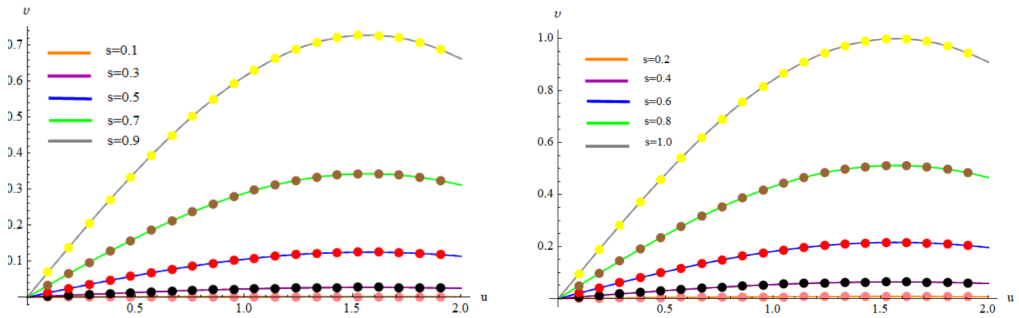

(a) $\hat{N} = 25, \psi = 0.5$ and $\Delta s = 1000$ (b) $\hat{N} = 25, \psi = 0.5$ and $\Delta s = 1000$

(c) $\hat{N} = 40, \psi = 0.8$ and $\Delta s = 0.002$ (d) $\hat{N} = 40, \psi = 0.8$ and $\Delta s = 0.002$

Figure 4. Exact and computational solutions for Example 7.2 at distinct time stages.

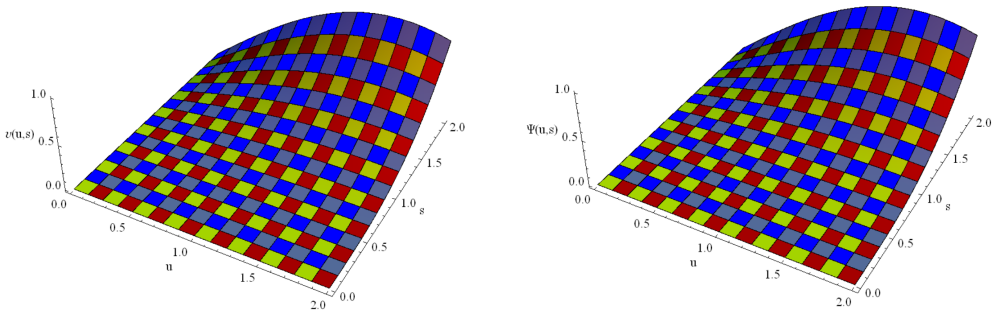

(a) Exact solution, (b) Approximate solution

Figure 5. 3D exact and approximate solution for Example 7.2, when $\hat{N} = 20$, $\psi = 0.5$, $\Delta s = 0.001$, and $s = 1$.

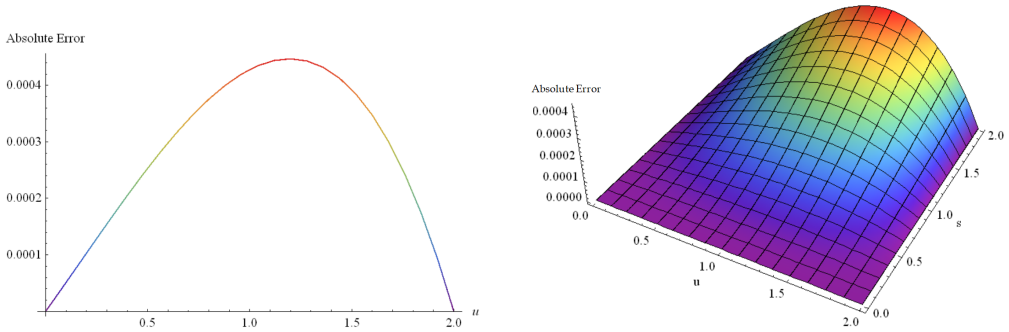

(a) 2D error graph (b) 3D error space-time graph

Figure 6. 2D and 3D error profiles for Example 7.2, when $\hat{N} = 25$, $\psi = 0.5$, $\Delta s = 0.001$, and $s = 1$.

8. Conclusions

An accurate numerical solution of the nonhomogeneous time-fractional BBM-Burger equation based on CBS functions has been determined in this study. For this purpose, CBS functions have been used to build up a collocation technique for the nonhomogeneous time-fractional BBM-Burger equation. The TF derivative has been approximated by the typical finite difference scheme and Atangana-Baleanu fractional operator, whereas the spatial derivative was discretized by using the θ-weighted scheme with CBS functions. Two test problems have been solved, and their graphical and numerical comparison uncovers that the proposed method is computationally very effective. The scheme has possessed the second order temporal and spatial convergence, as well as unconditionally stable. This method can be used to get efficient approximations for a large number of fractional differential equations. It has provided the results in the form of an improved solution for the problems for which there is no precise solution. This method offers effective solutions to numerous problems. In the future, we may consider the solution of higher dimensional and higher order BBM-Burger equations by using spline functions of higher degrees.

Author contributions

Muserat Shaheen: Methodology, writing-original draft; Muhammad Abbas: Supervision, methodology, writing-original draft; Miguel Vivas-Cortez: Software, formal analysis, writing-review & editing; M. R. Alharthi: Visualization, writing-review & editing; Y. S. Hamed: Software, formal analysis, writing-review & editing. All authors have read and approved the final version of the manuscript for publication.

Use of Generative-AI tools declaration

The authors declare that they have not used Artificial Intelligence (AI) tools in the creation of this article.

Acknowledgements

The authors would like to acknowledge the Deanship of Graduate Studies and Scientific Research, Taif University for funding this work.

Conflict of interest

The authors declare that they have no known competing financial interests or personal relationships that could have appeared to influence the work reported in this paper.

References

1. M. Xiao, W. X. Zheng, G. Jiang, J. Cao, Undamped oscillations generated by Hopf bifurcations in fractional-order recurrent neural networks with Caputo derivative, *IEEE T. Neur. Net. Lear.*, **26** (2015), 3201–3214. https://doi.org/10.1109/TNNLS.2015.2425734
2. N. Laskin, Fractional market dynamics, *Physica A*, **287** (2000), 482–492. https://doi.org/10.1016/S0378-4371(00)00387-3
3. V. D. Djordjevic, J. Jaric, B. Fabry, J. J. Fredberg, D. Stamenovic, Fractional derivatives embody essential features of cell rheological behavior, *Ann. Biomed. Eng.*, **31** (2003), 692–699. https://doi.org/10.1114/1.1574026
4. A. Babaei, H. Jafari, M. Ahmadi, A fractional order HIV/AIDS model based on the effect of screening of unaware infectives, *Math. Method. Appl. Sci.*, **42** (2019), 2334–2343. https://doi.org/10.1002/mma.5511
5. A. Babaei, M. Ahmadi, H. Jafari, A. Liya, A mathematical model to examine the effect of quarantine on the spread of coronavirus, *Chaos Soliton. Fract.*, **142** (2021), 110418. https://doi.org/10.1016/j.chaos.2020.110418
6. I. Podlubny, *Fractional differential equations*, San Diego: Academic, 1999.
7. J. H. He, Some applications of nonlinear fractional differential equations and their approximations, *Bull. Sci. Technol.*, **15** (1999), 86–90.

8. N. H. Tuan, Y. E. Aghdam, H. Jafari, H. Mesgarani, A novel numerical manner for two-dimensional space fractional diffusion equation arising in transport phenomena, *Numer. Meth. Part. D. E.*, **37** (2021), 1397–1406. https://doi.org/10.1002/num.22586
9. E. Atilgan, M. Senol, A. Kurt, O. Tasbozan, New wave solutions of time-fractional coupled Boussinesq-Whitham-Broer-Kaup equation as a model of water waves, *China Ocean Eng.*, **33** (2019), 477–483. https://doi.org/10.1007/s13344-019-0045-1
10. O. A. Arqub, Z. Odibat, M. A. Smadi, Numerical solutions of time-fractional partial integrodifferential equations of Robin functions types in Hilbert space with error bounds and error estimates, *Nonlinear Dynam.*, **94** (2018), 1819–1834. https://doi.org/10.1007/s11071-018-4459-8
11. C. I. Kondo, C. M. Webler, The generalized BBM-Burgers equations: Convergence results for conservation law with discontinuous flux function, *Appl. Anal.*, **95** (2016), 503–523. https://doi.org/10.1080/00036811.2015.1015524
12. J. Zhang, Z. Wei, L. Yong, Y. Xiao, Analytical solution for the time fractional BBM-Burger equation by using modified residual power series method, *Complexity*, **2018** (2018). https://doi.org/10.1155/2018/2891373
13. S. Abbasbandy, A. Shirzadi, The first integral method for modified Benjamin-Bona-Mahony equation, *Commun. Nonlinear Sci.*, **15** (2010), 1759–1764. https://doi.org/10.1016/j.cnsns.2009.08.003
14. A. Majeed, M. Kamran, M. K. Iqbal, D. Baleanu, Solving time fractional Burgers' and Fisher's equations using cubic B-spline approximation method, *Adv. Differ. Equ.*, **2020** (2020), 1–15. https://doi.org/10.1186/s13662-020-02619-8
15. A. Majeed, M. Kamran, N. Asghar, D. Baleanu, Numerical approximation of inhomogeneous time fractional Burgers-Huxley equation with B-spline functions and Caputo derivative, *Eng. Comput.*, **38** (2022), 885–900. https://doi.org/10.1007/s00366-020-01261-y
16. M. Shafiq, F. A. Abdullah, M. Abbas, A. S. M. Alzaidi, M. B. Riaz, Memory effect analysis using piecewise cubic B-spline of time fractional diffusion equation, *Fractals*, **30** (2022), 2240270. https://doi.org/10.1142/S0218348X22402708
17. M. Shafiq, M. Abbas, F. A. Abdullah, A. Majeed, T. Abdeljawad, M. A. Alqudah, Numerical solutions of time fractional Burgers' equation involving Atangana-Baleanu derivative via cubic B-spline functions, *Results Phys.*, **34** (2022), 105244. https://doi.org/10.1016/j.rinp.2022.105244
18. G. Arora, R. C. Mittal, B. K. Singh, Numerical solution of BBM-Burger equation with quartic B-spline collocation method, *Eng. Sci. Technol.*, **9** (2014), 104–116.
19. A. Umer, M. Abbas, M. Shafiq, F. A. Abdullah, M. D. L. Sen, T. Abdeljawad, Numerical solutions of Atangana-Baleanu time-fractional advection diffusion equation via an extended cubic B-spline technique, *Alex. Eng. J.*, **74** (2023), 285–300. https://doi.org/10.1016/j.aej.2023.05.028
20. R. M. Ganji, H. Jafari, A new approach for solving nonlinear Volterra integro-differential equations with Mittag-Leffler kernel, *Proc. Inst. Math. Mech.*, **46** (2020), 144–158. https://doi.org/10.29228/proc.24
21. H. Jafari, N. A. Tuan, R. M. Ganji, A new numerical scheme for solving pantograph type nonlinear fractional integro-differential equations, *J. King Saud Univ. Sci.*, **33** (2021), 101185. https://doi.org/10.1016/j.jksus.2020.08.029

22. R. K. Pandey, O. P. Singh, V. K. Baranwal, An analytic algorithm for the space-time fractional advection-dispersion equation, *Comput. Phys. Commun.*, **182** (2021), 1134–1144. https://doi.org/10.1016/j.cpc.2011.01.015
23. R. M. Ganji, H. Jafari, D. Baleanu, A new approach for solving multi variable orders differential equations with Mittag-Leffler kernel, *Chaos Soliton. Fract.*, **130** (2020), 109–405. https://doi.org/10.1016/j.chaos.2019.109405
24. X. Shen, A. Zhu, A Crank-Nicolson linear difference scheme for a BBM equation with a time fractional nonlocal viscous term, *Adv. Differ. Equ.*, **2018** (2018), 1–12. https://doi.org/10.1186/s13662-018-1815-4
25. C. Li, Linearized difference schemes for a BBM equation with a fractional nonlocal viscous term. *Appl. Math. Comput.*, **31** (2017), 240–250. https://doi.org/10.1016/j.amc.2017.05.022
26. A. Fakhari, D. Ganji, Ebrahimpour, Approximate explicit solutions of nonlinear BBM-Burger equations by homotopy analysis method and comparison with the exact solution, *Phys. Lett. A*, **368** (2007), 64–68. https://doi.org/10.1016/j.physleta.2007.03.062
27. L. Song, H. Zhang, Solving the fractional BBM-Burgers equation using homotopy analysis method, *Chaos Soliton. Fract.*, **40** (2009), 1616–1622. https://doi.org/10.1016/j.chaos.2007.09.042
28. S. Kumar, D. Kumar, Fractional modelling for BBM-Burger equation by using new homotopy analysis transform method, *J. Assoc. Arab Univ. Basic Appl. Sci.*, **16** (2014), 16–20. https://doi.org/10.1016/j.jaubas.2013.10.002
29. M. Shakeel, Q. M. U. Hassan, J. Ahmad, T. Naqvi, Exact solutions of the time fractional BBM-Burger equation by novel expansion method, *Adv. Math. Phys.*, **2014** (2014), 181594. https://doi.org/10.1155/2014/181594
30. B. Hong, Assorted exact explicit solutions for the generalized Atangana's fractional BBM-Burgers equation with the dissipative term, *Front. Phys.*, **10** (2022), 1071200. https://doi.org/10.3389/fphy.2022.1071200
31. J. Zhang, Z. Wei, L. Yong, Y. Xiao, Analytical solution for the time fractional BBM-Burger by using modified residual power series method, *Complexity*, **2018** (2018). https://doi.org/10.1155/2018/2891373
32. H. M. Salih, L. N. M. Tawfiq, Z. R. Yahya, Using cubic trigonometric B-spline method to solve BBM-Burger equation, *IWNEST Conf. P.*, **2** (2016), 1–9.
33. S. Arora, R. Jain, V. K. Kukreja, Solution of Benjamin-Bona-Mahony-Burgers equation using collocation method with quintic Hermite splines, *Appl. Numer. Math.*, **154** (2020), 1–16. https://doi.org/10.1016/j.apnum.2020.03.015
34. S. B. G. Karakoc, K. K. Ali, Theorical and computational structure on solitary wave solution of Benjamin Bona Mahony-Burger equation, *Tbilisi Math. J.*, **14** (2014), 33–50. https://doi.org/10.32513/tmj/19322008120
35. K. Omrani, M. Ayadi, Finite difference discretization of the Benjamin-Bona-Mahony-Burger equation, *Numer. Meth. Part. D. E.*, **24** (2008), 239–248. https://doi.org/10.1002/num.20256
36. S. B. G. Karakoc, S. K. Bhowmik, Galerkin finite element solution for Benjamin-Bona-Mahony-Burgers equation with cubic B-splines, *Comput. Math. Appl.*, **77** (2019), 1917–1932. https://doi.org/10.1016/j.camwa.2018.11.023

37. A. Majeed, M. Kamran, M. Abbas, M. Y. B. Misro, An efficient numerical scheme for the simulation of time-fractional nonhomogeneous Benjamin-Bona-Mahony-Burger model, *Phys. Scripta*, **96** (2021), 084002. https://doi.org/10.1088/1402-4896/abfde2
38. J. Lin, L. Shi, S. Reutskiy, J. Lu, Numerical treatment of multi-dimensional time-fractional Benjamin-Bona-Mahony-Burgers equations in arbitrary domains with a novel improvised RBF-based method, *Comput. Math. Appl.*, **167** (2024), 178–198. https://doi.org/10.1016/j.camwa.2024.05.018
39. M. Kamran, M. Abbas, A. Majeed, H. Emadifar, T. Nazir, Numerical simulation of time fractional BBM-Burger equation using cubic B-Spline functions, *J. Funct. Space.*, **2022** (2022), 2119416. https://doi.org/10.1155/2022/2119416
40. H. Salih, Solution BBM-Burger equation via quartic trigonometric B-spline approach, *J. Phys. Conf. Ser.*, **1879** (2021), 022109. https://doi.org/10.1088/1742-6596/1879/2/022109
41. L. Mohan, A. Prakash, Stability and numerical analysis of fractional BBM-Burger equation and fractional diffusion-wave equation with Caputo derivative, *Opt. Quant. Electron.*, **56** (2024), 26. https://doi.org/10.1007/s11082-023-05608-9
42. V. Kumar, Nonlinear waves and modulation instability in the generalized Burger-BBM equation, *Nonlinear Sci.*, **2** (2025), 100013. https://doi.org/10.1016/j.nls.2025.100013
43. A. E. shenawy, M. E. Gamel, D. Reda, Troesch's problem: A numerical study with cubic trigonometric B-spline method. *Part. Differ. Eq. Appl. Math.*, **10** (2024), 100694. https://doi.org/10.1016/j.padiff.2024.100694
44. M. E. Gamel, W. E. Bashbashy, A. E. Shenawy, Numerical solutions for the time-dependent Emden-Fowler-type equations by B-spline method, *Appl. Math.*, **5** (2014), 593–600. https://doi.org/10.4236/am.2014.54056
45. A. Atangana, D. Baleanu, New fractional derivatives with nonlocal and non-singular kernel: Theory and application to heat transfer model, *Therm. Sci.*, **20** (2016), 757–763. https://doi.org/10.2298/TSCI160111018A
46. M. Partohaghighi, M. Inc, M. Bayram, D. Baleanu, On numerical solution of the time fractional advection-diffusion equation involving Atangana-Baleanu-Caputo derivative, *Open Phys.*, **17**, (2019), 816-822. https://doi.org/10.1515/phys-2019-0085
47. J. R. Poulin, *Calculating infinie series using parsevals identity (master thesis)*, The University of Maine, Orono, 2020.
48. M. Shafiq, M. Abbas, H. Emadifar, A. S. Alzaidi, T. Nazir, F. A. Abdullah, Numerical investigation of the fractional diffusion wave equation with exponential kernal via cubic B-spline approach, *PLoS One*, **18** (2023), 0295525. https://doi.org/10.1371/journal.pone.0295525
49. M. Shafiq, M. Abbas, K. M. Abualnaja, M. J. Huntul, A. Majeed, T. Nazir, An efficient technique based on cubic B-spline functions for solving time-fractional advective diffusion equation involving Atangana-Baleanu derivative, *Eng. Comput.*, **38** (2022), 901–917. https://doi.org/10.1007/s00366-021-01490-9
50. S. G. Rubin, R. A. J. Graves, A cubic spline approximation for problems in fluid mechanics, *NASA STI/Recon Tech. Rep. N*, **75** (1975), 33345.

51. M. Yaseen, M. Abba, A. I. Ismail, T. Nazir, A cubic trigonometric B-spline collocation approach for the fractional sub-diffusion equations, *Appl. Math. Comput.*, **293** (2017), 311–319. https://doi.org/10.1016/j.amc.2016.08.028

52. S. T. M. Din, T. Akram, M. Abbas, A. T. Ismail, N. H. M. Ali, A fully implicit finite difference scheme based on extanded Cubic B-spline for time fractional advective diffusion equation, *Adv. Differ. Equ.*, **2018** (2018), 1–17. https://doi.org/10.1186/s13662-018-1537-7

53. C. A. Hall, Optimal erroe bounds for cubic B-spline interpolation. *J. Approx. Theory*, **16** (1976) 105–122. https://doi.org/10.1016/0021-9045(76)90040-X

54. C. D. Boor, On the convergence of odd-degree spline interpolation, *J. Approx. Theory*, **1** (1968), 452–463. https://doi.org/10.1016/0021-9045(68)90033-6

55. S. Yadav, R. K. Pandey, A. K. Shukla, Numerical approximation of Atangana-Baleanue Caputo derivative and its applications, *Chaos Soliton. Fract.*, **118** (2019), 58–64. https://doi.org/10.1016/j.chaos.2018.11.009

AIMS Press

© 2025 the Author(s), licensee AIMS Press. This is an open access article distributed under the terms of the Creative Commons Attribution License (https://creativecommons.org/licenses/by/4.0)